




Article

Properties of Laser-Clad Stainless Steel–Ni/WC Double-Layer Coatings

Ruipeng Zhang ¹, Yuhong Liao ¹, Qingyi Sai ^{2,*}, Shuwen Wang ^{1,*}, David Barton ³ and Mingwen Bai ³

¹ College of Mechanical Engineering, University of Shanghai for Science and Technology, Shanghai 200093, China; zhangruipeng199810@163.com (R.Z.); helenlyhr@163.com (Y.L.)

² College of Energy and Power Engineering, University of Shanghai for Science and Technology, Shanghai 200093, China

³ School of Mechanical Engineering, University of Leeds, Leeds LS2 9JT, UK; d.c.barton@leeds.ac.uk (D.B.); m.bai2@leeds.ac.uk (M.B.)

* Correspondence: saiqingyi@163.com (Q.S.); shuwenwang66@163.com (S.W.)

Abstract: In order to improve the wear and corrosion resistance and enhance the tribological and mechanical properties of gray cast iron, the laser surface cladding technique was employed to fabricate double-layer coatings with different Ni/WC ratios on the surface of gray cast iron. The effects of laser processing parameters and the type of Ni-based alloy on the microstructure and properties of the gray cast iron matrix and laser-clad layer were investigated. A 316L stainless steel transition layer was introduced between the gray cast iron substrate and the Ni/WC coating to prevent the cladding layer from cracking. The tribological and mechanical properties of the laser-clad coatings were characterized with various tests at the macro- and micro-scales; the residual stresses on the coating surfaces were measured, and electrochemical tests were also carried out. The microstructures of the clad layers were analyzed by scanning electron microscope (SEM) and X-ray diffraction (XRD). The results show that the laser-clad layers exhibit excellent vibration and noise reduction performance, which is partially due to the reduction and stabilization of the coefficients of friction (COFs) and the high levels of compressive residual stress on the surface of the laser-clad layers. The wear and corrosion resistance of the laser-clad layers are significantly improved, and the maximum wear loss of the laser-clad coating was about only 5% of that of the unclad gray cast iron substrate. This research has significance for the laser surface modification of cast iron, steel, and other metals, which is an increasingly important topic, especially in the automotive friction brake industry.

Keywords: laser cladding; vibration and noise; friction and wear; corrosion; Ni/WC; gray cast iron



Citation: Zhang, R.; Liao, Y.; Sai, Q.; Wang, S.; Barton, D.; Bai, M.

Properties of Laser-Clad Stainless Steel–Ni/WC Double-Layer Coatings.

Coatings **2024**, *14*, 1054. <https://doi.org/10.3390/coatings14081054>

Academic Editor: Rafael Comesaña

Received: 19 July 2024

Revised: 13 August 2024

Accepted: 15 August 2024

Published: 18 August 2024



Copyright: © 2024 by the authors. Licensee MDPI, Basel, Switzerland. This article is an open access article distributed under the terms and conditions of the Creative Commons Attribution (CC BY) license (<https://creativecommons.org/licenses/by/4.0/>).

1. Introduction

In recent years, laser surface modification techniques have been more and more popular for the improvement of functional surfaces. For example, laser cladding has been widely recognized as a super green technique for surface coating because it has the advantages of high-strength metallurgical bonding, small heat-affected zone and deformation, fine-grain size with high density, a range of coating materials that can be used, and environmental friendliness [1].

Comprehensive research on the properties of laser-clad coatings in various areas has been carried out in the last decades. In tribological studies, anti-wear coatings have been laser clad on various materials, such as Invar alloy [2], Inconel 718 [3], carbon steel [4–8], stainless steel [9], magnesium alloy [10], gray cast iron, and ductile cast iron [11]. In order to study their wear resistance mechanisms, the microstructures and wear behavior of laser-clad coating layers were investigated [12–14]. The results show that composite coatings employing more than one constituent material exhibit better micro-hardness and wear resistance [6]. The addition of Mo [13], Co [15], Ti [9], and other elements can improve both the micro-hardness and wear resistance of the coatings.

In an anti-corrosion study of laser-clad coatings, experimental results showed that the corrosion resistance of a Ni-WC [10] composite coating was better than that of a single material coating. The addition of Ni [16], In [17], WC [8], and SiC [6] can effectively improve the corrosion resistance of the coatings, as well as the tribological and mechanical properties.

The laser-cladding process parameters also have a significant effect on the properties of such coatings, and this has been investigated by many researchers. Khorram et al. [3] found that the laser frequency and pulse width had a positive effect on the thickness of the laser-clad layer, but the cladding angle and dilution rate had a negative effect on the thickness and hardness of the clad bead. Caneda et al. [4] studied the effects of the laser cladding parameters on the dilution rate, microstructure, and mechanical properties in order to obtain a coating with high hardness and good wear resistance. Riquelme et al. [18] analyzed the influence of different process control parameters on the preparation of an Al/SiC composite coating on the surface of AA6082 aluminum alloy by laser cladding, and the Taguchi DOE method [19] was used to reduce the number of experiments required. By optimizing the laser control parameters, the height and width of the coating and the quality of the substrate-coating interface were improved, and the depth of the melted zone was minimized [18]. Arias-González et al. [11] studied the relationship between the laser processing parameters and the geometry of a single laser trajectory and determined the optimum processing parameters for fabricating the coating. Mahade et al. [20] used HVOF (High-velocity Oxy-Fuel) and HVOF (High-Velocity Air Fuel) thermal spraying methods to fabricate Rockit-401 crystalline iron-based coatings and studied the effects of deposition methods and process conditions on microstructure, porosity, hardness, and phase composition. The results provided clues for understanding the processing technology, wear behavior, and wear mechanism of a durable, high-performance coating.

Different cladding materials and processes have been found to have significant effects on the surface modification of gray cast iron. Tonolini et al. [21] used two different powders (martensitic stainless steel powder and the same powder enhanced by adding tungsten carbide spherical particles) for laser cladding. Compared with the conventional gray cast iron material and a single material stainless steel coating, the coating containing tungsten carbide had better wear resistance. This suggests that stainless steel coatings reinforced by hard particles can be used to improve the wear resistance of cast iron brake discs. Manoj et al. [22] laser clad gray cast iron substrates with two iron-based (AISI 4140 and SS420) powders and one cobalt-based powder (Stellite 6). Tribological test results showed that the COFs of AISI 4140 and Stellite 6 coatings were stable, but the COFs of SS420 coatings were not stable due to the serious damage occurring on the coating surfaces; the AISI 4140 coating was found to be the most wear-resistant coating. Ouyang et al. [23] laser clad multi-layers on the surfaces of nodular and gray cast iron. Experimental results showed that the Ni-based coating had lower internal stress than that of Fe- and Co-based coatings. Therefore, Ni-based coating with lower cladding stress can be used as a transition layer to avoid laser cladding defects. Li et al. [24] laser clad composite coating layer of Invar 36 alloy powder and NiCu alloy powder for the anti-corrosion protection of ductile iron. This study found that the use of cladding alloys with low thermal expansion characteristics to repair ductile cast iron surfaces can reduce the shrinkage of the cladding layer, thereby reducing residual stress and cracks. In order to solve the problem of brittleness of the bonding interface, Liu et al. [25] used the laser multi-layer cladding method to prepare a nickel-based alloy coating on the surface of compacted graphite iron and studied the effect of dilution rate on the microstructure and corrosion behavior of the coating. With the increase in Ni and Cr concentration in the coating, the oxygen vacancies decreased during the corrosion process, and the corrosion resistance was improved.

The wear, corrosion, and NVH (noise, vibrations, and harshness) of brake discs have become the most critical problems to be solved for automotive brake manufacturers over the last decades. In particular, due to strict regulations introduced in Europe and elsewhere to control particulate emissions from brakes, there is an urgent need to develop surface treatments for cast iron brake discs which give high durability, reduced wear, and good

anti-corrosion properties. In this work, the surface modification of gray cast iron samples was carried out by laser-cladding technology. The effects of different laser processing parameters and various Ni-based alloys on the internal micro-structures and properties of the laser-clad coatings were investigated. Optimal laser-cladding parameters and powder ratios were used for a composite Ni/WC laser cladding to improve the physical and chemical properties, wear resistance, vibration, and noise reduction performance of the laser-clad layer on the cast iron substrates and to explore the corrosion resistance of the Ni-based coatings in a highly corrosive environment.

2. Material and Methodology

2.1. Laser Cladding Materials

In this study, based on our previous experience of laser cladding Ni625/WC composite powders on gray cast iron HT250 [26], four different Ni-based alloys (Ni35, Ni45, Ni60, and Ni625) were used as the main laser-cladding materials. The particle sizes of these four Ni-based alloy powders were 150–325 mesh for Ni35 and Ni60 with a hardness of 35 HRC and 60 HRC, respectively, and 80–270 mesh for Ni45 and Ni625 with a hardness of 45 HRC and 56–63 HRC, respectively. The particle size of the WC powder was 150–325 mesh with a hardness of 80 HRC. Table 1 gives the chemical composition of the Ni35, Ni45, Ni60, and Ni625 alloy powders, whilst Table 2 shows the composition of the WC powder. Figure 1 displays the microscopic morphologies of all the powders employed in this study. SEM-EDS analyses of the Ni powders can be found in Yuan [27] and Chen [28].

Table 1. Chemical composition of Ni-based alloy powders [27,28].

	C	Cr	Si	Fe	Ni	B	Mo	Co	Mn	P	S	Nb	Al	Ti
Ni35	<0.3	8.0–15.0	2.8–3.8	<8	70.4–79.4	1.5–2.5								
Ni45	0.2–0.6	2.0–7.0	3.0–4.5	<8	76.9–84.8	2.0–3.0								
Ni60	0.5–1.1	14–20	3.5–5.5	<15	65–80	3.0–4.5	0.503							
Ni625	0.1	23	0.5	5	54.92		10	1	0.5	0.015	0.015	4.15	0.4	0.4

Table 2. Chemical composition of WC powder.

WC	Al	Ca	Fe	K	Mg	Mo	Na	S	Si
≥99.8	0.002	0.002	0.02	0.0015	0.002	0.01	0.0015	0.002	0.003

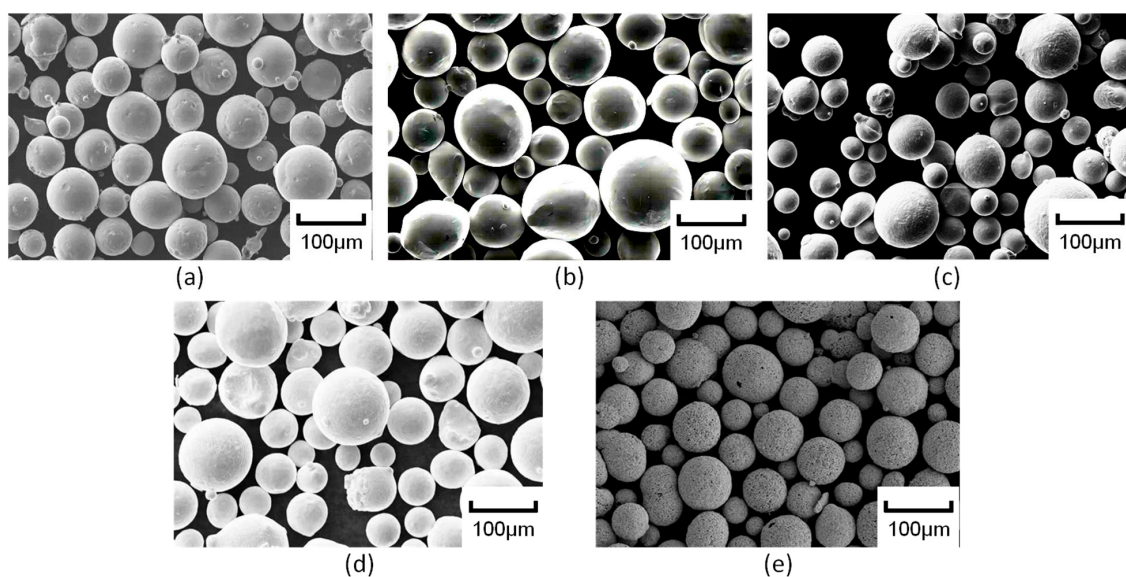


Figure 1. Microscopic morphology of laser-cladding powders. (a) Ni35; (b) Ni45; (c) Ni60; (d) Ni625; (e) WC.

2.2. Laser-Cladding Equipment

A TruDisk4002 disc laser machine (manufactured by TRUMPF (China) Co., Ltd., Beijing, China) with a needle powder feeding nozzle was employed for the laser cladding in this study. This machine utilizes a highly flexible six-axis mechanical arm, and the output power is continuously adjustable within a power range of 80–4000 W. During the laser cladding process, argon was used as a protective gas to prevent oxidation. This laser-cladding system is illustrated in Figure 2.

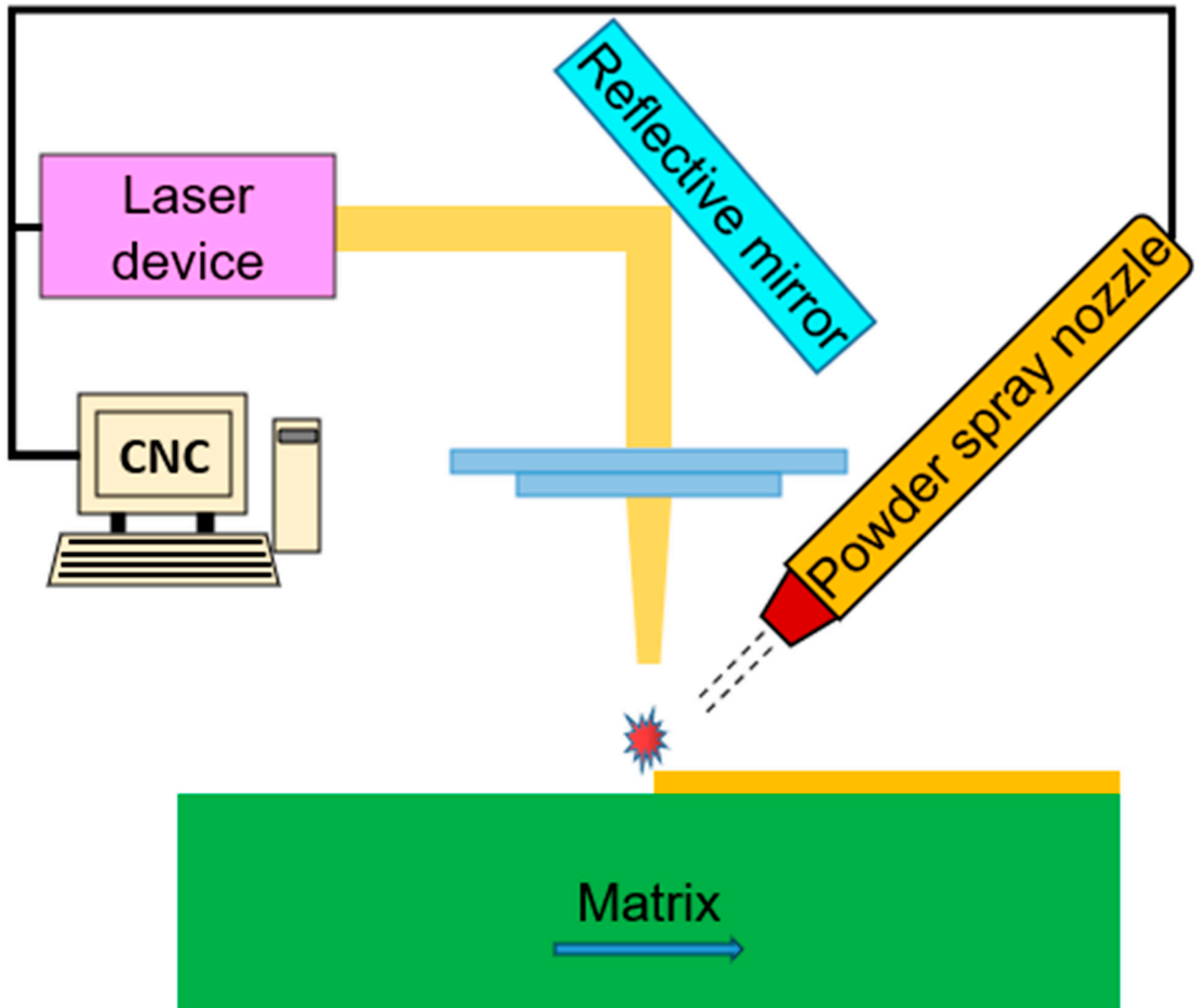


Figure 2. Schematic illustration of laser-cladding system.

2.3. Laser-Cladding of Double-Layer Coatings

In order to prevent the laser-clad Ni-WC composite coatings, particularly the Ni60/WC composite coatings, from cracking, a laser-clad 316L stainless steel transition layer between the Ni/WC alloy and the gray cast iron substrate was introduced in this study. Because the Ni-based alloy has excellent corrosion resistance and the WC has excellent wear resistance, the laser-clad Ni/WC coatings were designed to be excellent in both anti-wear and corrosion protection. The laser-cladding parameters for the 316L stainless steel interlayer are shown in Table 3, and the laser-cladding parameters for the Ni-based alloy coatings

are listed in Table 4. Two samples were laser-clad for each coating composition and set of processing parameters.

Table 3. Parameters for laser cladding of 316L stainless steel interlayer.

Laser Power (W)	Feed Speed (mm/min)	Rotating Speed of Powder Feeder (r/min)	Protective Gas Flow (L/min)	Powder Feed Gas Flow (L/min)
1100	600	1.5	15.0	5.0

Table 4. Parameters for laser cladding of Ni-based/WC composite surface layer.

No.	Laser Power (W)	Feed Speed (mm/min)	Rotating Speed of Powder Feeder (r/min)	Protective Gas Flow (L/min)	Powder Feed Gas Flow (L/min)	WC Content (%)	Ni Content (%) and Type	
1	1100	580	4.9	15.4	5.8	40	60	Ni35
2	1400	660	4.4	15.3	4.2	30	70	
3	2000	600	4.5	15.1	5.4	10	90	
4	1100	580	4.9	15.4	5.8	40	60	Ni45
5	1400	660	4.4	15.3	4.2	30	70	
6	2000	600	4.5	15.1	5.4	10	90	
7	1100	580	4.9	15.4	5.8	40	60	Ni60
8	1400	660	4.4	15.3	4.2	30	70	
9	2000	600	4.5	15.1	5.4	10	90	
10	1100	580	4.9	15.4	5.8	40	60	Ni625
11	1400	660	4.4	15.3	4.2	30	70	
12	2000	600	4.5	15.1	5.4	10	90	

The laser-clad surfaces were finally polished by means of a diamond grinding wheel. Figure 3a,b show images of the laser-clad double-layer coated specimens (1#: specimen 1; 2#: specimen 2; 3#: specimen 3; 4#: specimen 4; 5#: specimen 5; 6#: specimen 6) before and after surface polishing, respectively. Figure 3c illustrates a schematic cross-section of the laser-clad double-layer samples, showing the nominal thicknesses of the different layers.

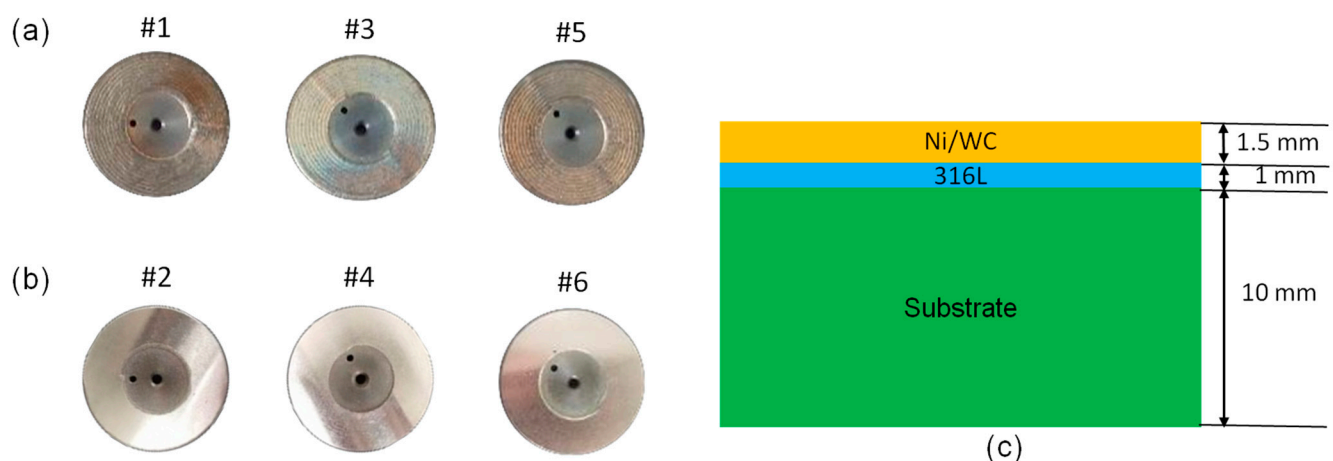


Figure 3. Laser-clad specimens. (a) before surface polishing; (b) after surface polishing; (c) illustration of cross-section through specimen.

2.4. Experimental Methodology

2.4.1. Friction and Wear Tests

The UMT-TriboLab friction and wear testing machine (Bruker Co., Ltd., Billerica, MA, USA) was employed for the tribological tests, as illustrated in Figure 4, where the lower rotational frictional contact part is a cast iron disc 70 mm in diameter with or without

a laser-clad coating layer while the upper stationary frictional counterpart is a stainless steel ball with a diameter of 5 mm. In all tribological tests, the normal load was 20 N; the rotational, linear speed at the steel ball contact radius was 1 m/s; and the dry frictional sliding distance was 100 m.

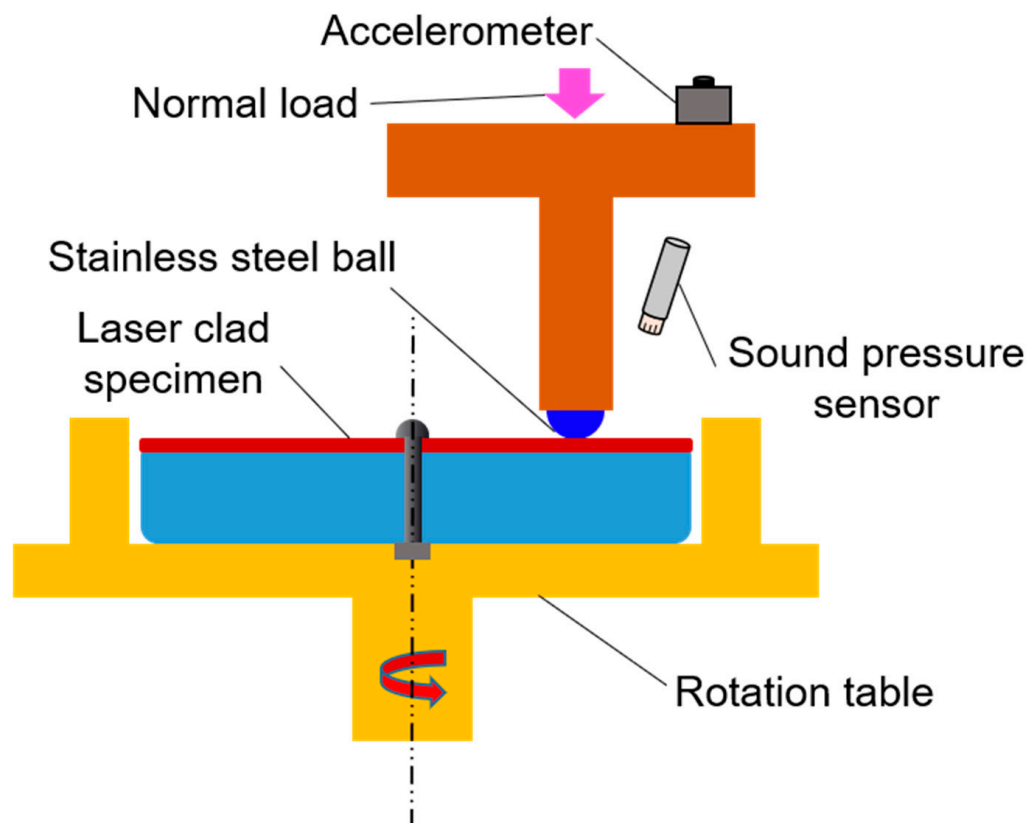


Figure 4. Schematic illustration of tribo-dynamical testing with the UMT-TriboLab machine.

2.4.2. Vibration and Noise Measurements

A vibration accelerometer (INV9832-50, BOINV, Beijing, China) and a sound pressure sensor (INV9202, BOINV, Beijing, China) were installed near the friction pair (as shown in Figure 4) to collect the frictional vibration and noise signals. A data acquisition and signal processing (DASP) system developed by Beijing Oriental Institute of Noise and Vibration (BOINV) was employed for the vibration and noise data acquisition and subsequent analysis.

2.4.3. Residual Stress Measurements

A TEC 4000 X-ray diffraction system (TEC Materials Testing, Knoxville, TN, USA) was employed for the residual stress measurements. The radial and tangential residual stresses at three points on the surface of each laser-clad specimen were measured by the $\sin^2 \psi$ method [29], and the average residual stresses were obtained. The three measured points were evenly distributed on the unworn surface of the laser-clad samples. The same method was used to measure the residual stresses on the cast iron surfaces without laser cladding.

2.4.4. Electrochemical Corrosion Tests

The electrochemical experiments were carried out with the Gamry Electrochemical Station (Model Interface 1010E, Gamry, Warminster, PA, USA). The equipment used in this electrochemical corrosion experiment is listed in Table 5. The anodic and cathodic polarization curves of laser-clad cast iron samples were measured by the potentiodynamic scanning method. During these experiments, the temperature was maintained at room temperature of 26 °C. The sample immersed in about 3 L of 3.5% NaCl electrolyte solution

for 2 h was used as the working electrode, a metal platinum sheet was used as the auxiliary electrode, and a saturated calomel electrode was used as the reference electrode. The scanning rate was 1 mV/s, and the voltage range was -1.2 V to $+0.5$ V.

Table 5. Equipment used in the electrochemical experiments.

Equipment	Model	Manufacturer
Electronic balance	ME104E	Beijing Grand Boyu Technology, Beijing, China
Magnetic stirrer	MS7-H550-Pro	Qingdao Juchuang Environmental Protection Group, Qingdao, China
Supersonic cleaner	KQ-250 DB	Kunshan Ultrasonic Instruments, Kunshan, China
Constant-temperature water tank	HC-1	Qingdao Mingbo Environmental Protection Technology, Qingdao, China
Gamry electrochemical workstation	Interface1010E	Gamry Instruments, Warminster, PA, USA

2.4.5. Micro-Structure Analysis

The microscopic morphology of the Ni/WC laser-clad layers was observed and analyzed by the scanning electron microscope (SEM, Hitachi S-3400N, Hitachi, Ltd., Tokyo, Japan). In addition, an X-ray diffractometer (XRD, D2 PHASER, Bruker Technology Co., Ltd., Billerica, MA, USA) was used to analyze the phase changes of the laser-clad layers.

3. Results and Discussion

3.1. Friction

Figure 5 presents the coefficients of friction (COFs) obtained from the ball-on-disc tribological tests described in Section 2.4.1. It can be seen from Figure 5 that the COFs of the unclad cast iron specimen increased significantly from 0.12 to 0.32 within 60 s of starting the sliding contact. In contrast, the COFs of all the laser-clad coatings are significantly lower and generally more stable. Figure 5 also shows that the COFs of laser-clad specimens 1–9 and 11 are about 0.12 and very stable during the whole testing period, but the COFs of specimens 10 and 12 have increased to about 0.16 by the end of the testing period.

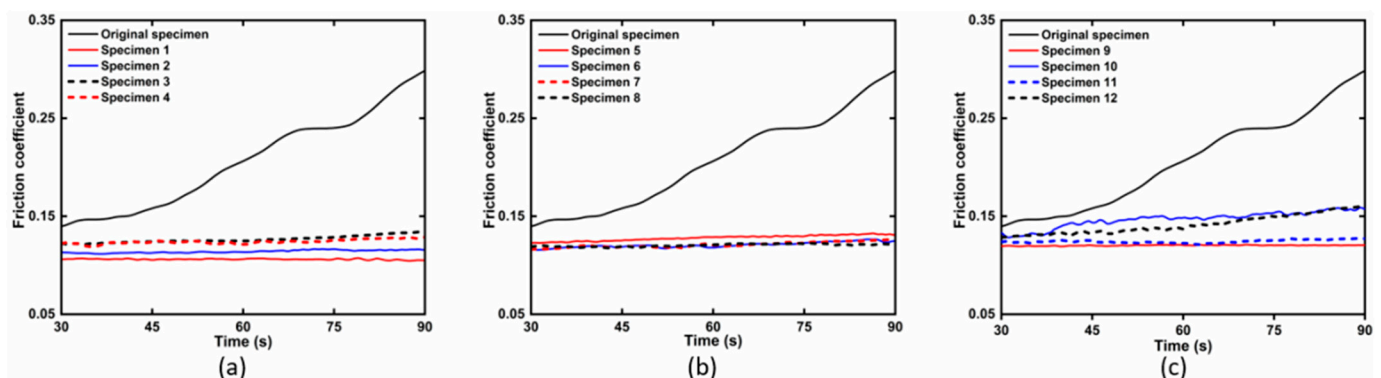


Figure 5. Measured COFs of specimens. (a) specimens 1–4 and original; (b) specimens 5–8 and original; (c) specimens 9–12 and original.

3.2. Wear

Figure 6 demonstrates the surface topographies of the 13 specimens measured using the BRUKER white light interferometer (Bruker Co., Ltd., Billerica, MA, USA) after tribological tests. It can be observed from Figure 6 that the wear marks on the surface of the original unclad cast iron specimen are significantly wider and deeper than those of the laser-clad specimens. It can also be seen from Figure 6 that the wear scars on the surface of specimen 10 are significantly wider and deeper than those of the other laser-clad specimens.

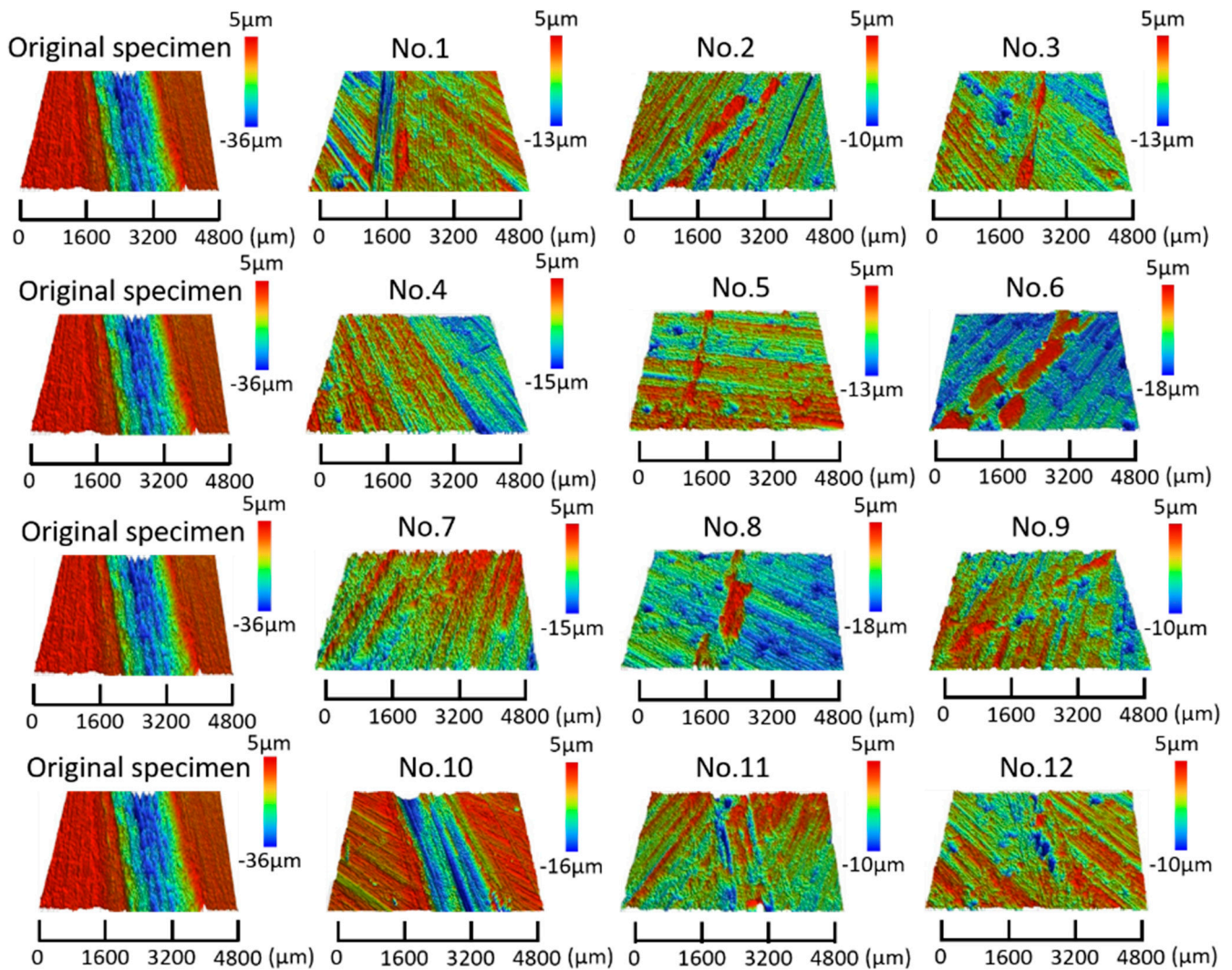


Figure 6. Surface topography of specimens measured with the white light interferometer after tribological tests.

Figure 7 presents the calculated wear volume of the 13 specimens after tribological tests. It can be seen from Figure 7 that the wear loss of the original unclad specimen is significantly larger than that of the laser-clad specimens, which may be linked to the fact that the COF of this original specimen significantly increased with increasing sliding distance. It can be seen that the wear loss of specimens 10 and 12 is significantly larger than that of the other laser-clad specimens, which may be linked to their increasing COFs with sliding distance. Among specimens 1–9, the wear loss of specimen 7 is the smallest, being only about 7% of the wear loss of the original specimen, indicating that specimen 7 has the best wear resistance as well as very stable COFs.

From a cross-reference between the wear results in Figure 7 and the process parameters in Table 3, it can be observed that, for the Ni35/WC and Ni625/WC composite coatings (specimens 1–3 and 10–12), the wear loss decreased with the increase in laser-cladding power and with the decrease in WC content. For the Ni45/WC composite coatings (specimens 4–6), the wear loss increased with the increase in laser power and the decrease in WC content. However, the laser power and WC content appear to have no significant effect on the wear loss of the Ni60/WC composite coating specimens 7–9.

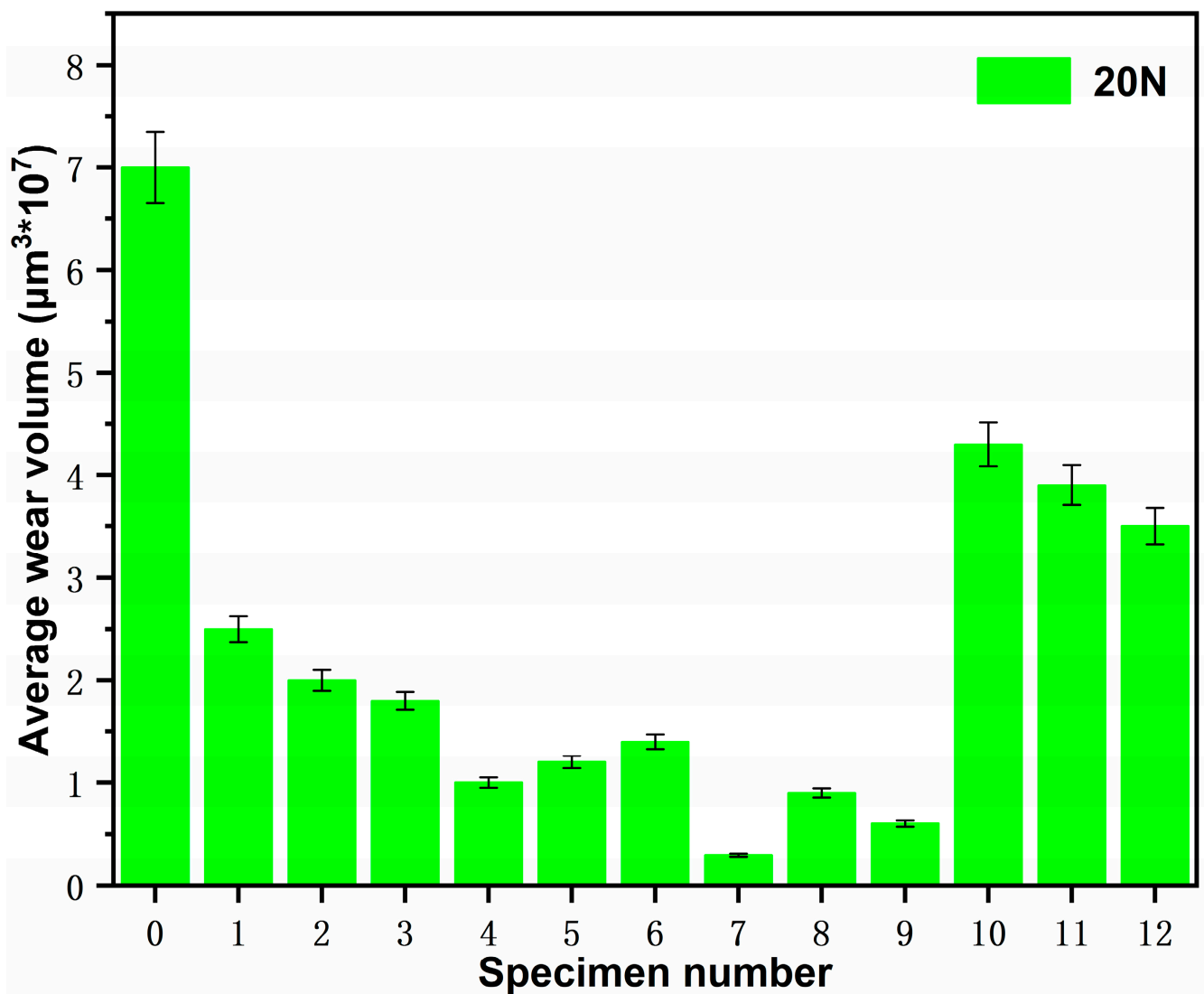


Figure 7. Average wear volume of specimens with and without laser-clad coating.

3.3. Vibrations

As shown in Figure 8, the friction-induced peak vibration acceleration between the unclad cast iron specimen 0 and the stainless steel ball is 32.54 m/s^2 when the applied normal force is 20 N, and the linear sliding speed is 1 m/s. The vibrations of specimen 0 mainly appear across the frequency range up to 4 kHz, but the vibrations of the laser-clad specimens mainly occur below 2 kHz, and their peak amplitudes are significantly reduced. For the specimens with laser-clad Ni35/WC and Ni45/WC coatings, specimens 3 and 5 appear to have the best damping effect with peak vibration amplitudes of 16.36 m/s^2 and 13.13 m/s^2 , respectively. For the specimens with laser-clad Ni60/WC and Ni625/WC coatings, specimens 9 and 12 have the best damping effect with a peak vibration acceleration of 9.40 m/s^2 and 3.98 m/s^2 , respectively. It is obvious that the Ni625/WC coatings have the best overall vibration-damping effect, while the Ni35/WC coatings have the worst damping effect among the four kinds of Ni-based coatings. However, all the Ni-based coatings have lower acceleration amplitudes and, therefore, more effective vibration-damping properties than those of the unclad gray cast iron. This, of course, is also related to the lower and more stable COFs of the laser-clad samples.

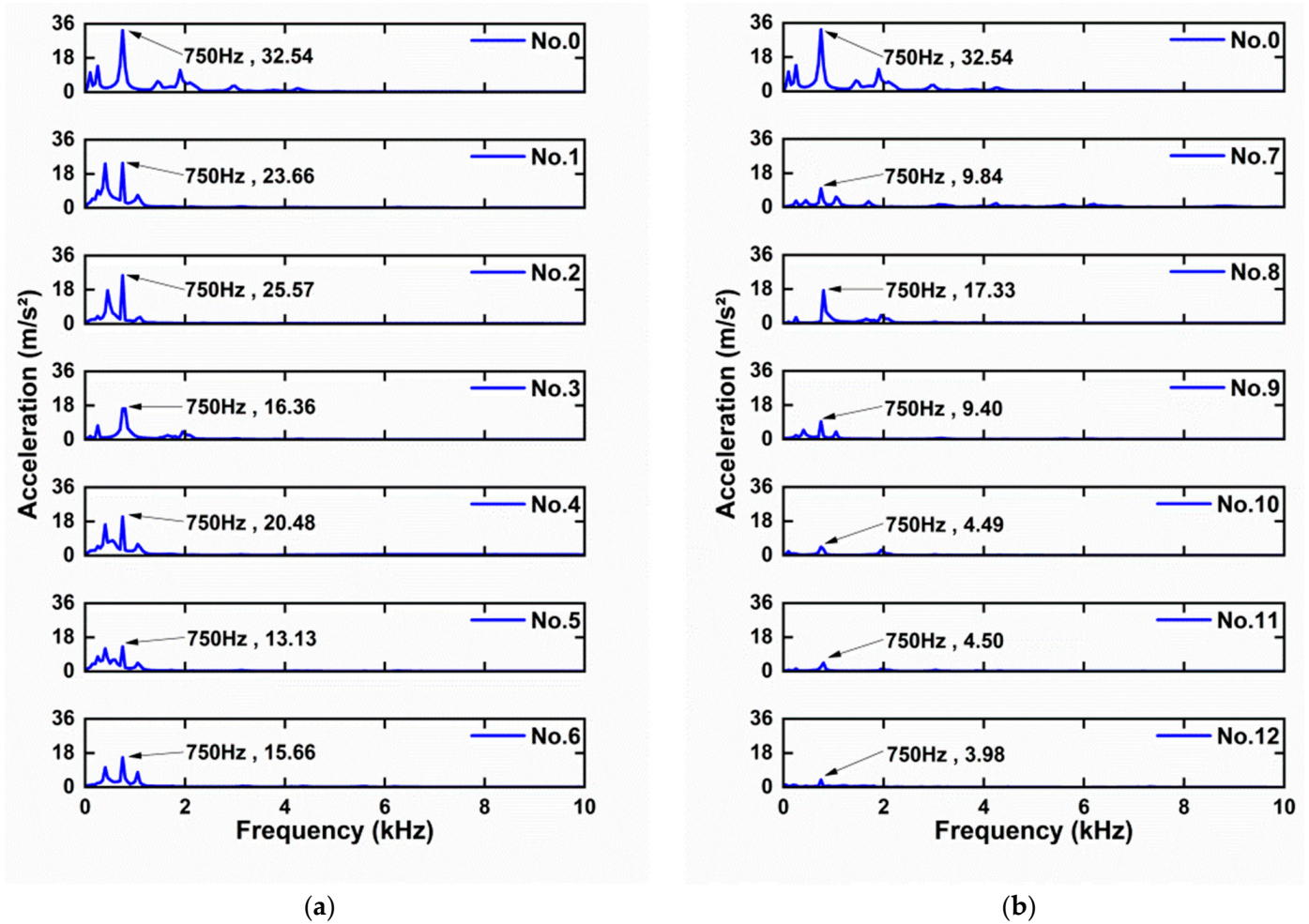


Figure 8. Frictional vibration spectra of specimens. (a) Unclad specimen 0 and clad specimens 1–6; (b) unclad specimen 0 and clad specimens 7–12.

3.4. Noise

Figure 9 presents the frictional noise spectra of the unclad specimen 0 and laser-clad specimens 1–12. It can be seen that frictional noise occurs at frequencies up to 6 kHz for unclad specimen 0 and clad specimen 1, but for specimens 2–12, frictional noise only occurs at frequencies below 2 kHz. The peak noise of the unclad specimen 0 occurs at 1.9 kHz, and its corresponding sound pressure is 0.67 Pa. The friction-induced noise pressure from the 12 laser-clad specimens is significantly reduced compared with this value. Specimen 12 demonstrates the best performance in noise reduction with a peak sound pressure of 0.05 Pa, while specimen 1 has the worst noise reduction effect with a peak sound pressure of 0.28 Pa, followed by specimens 2 and 3.

Considering that specimens 10–12 have the best performance in both vibration and noise reduction and that specimens 1–3 have the worst performance, it may be concluded that Ni625/WC is the best laser-cladding composite material for reducing vibration and noise effects in this study; the Ni35/WC coating is the least effective and the results for the Ni45/WC and Ni60/WC coatings are between those for the Ni625/WC and Ni35/WC.

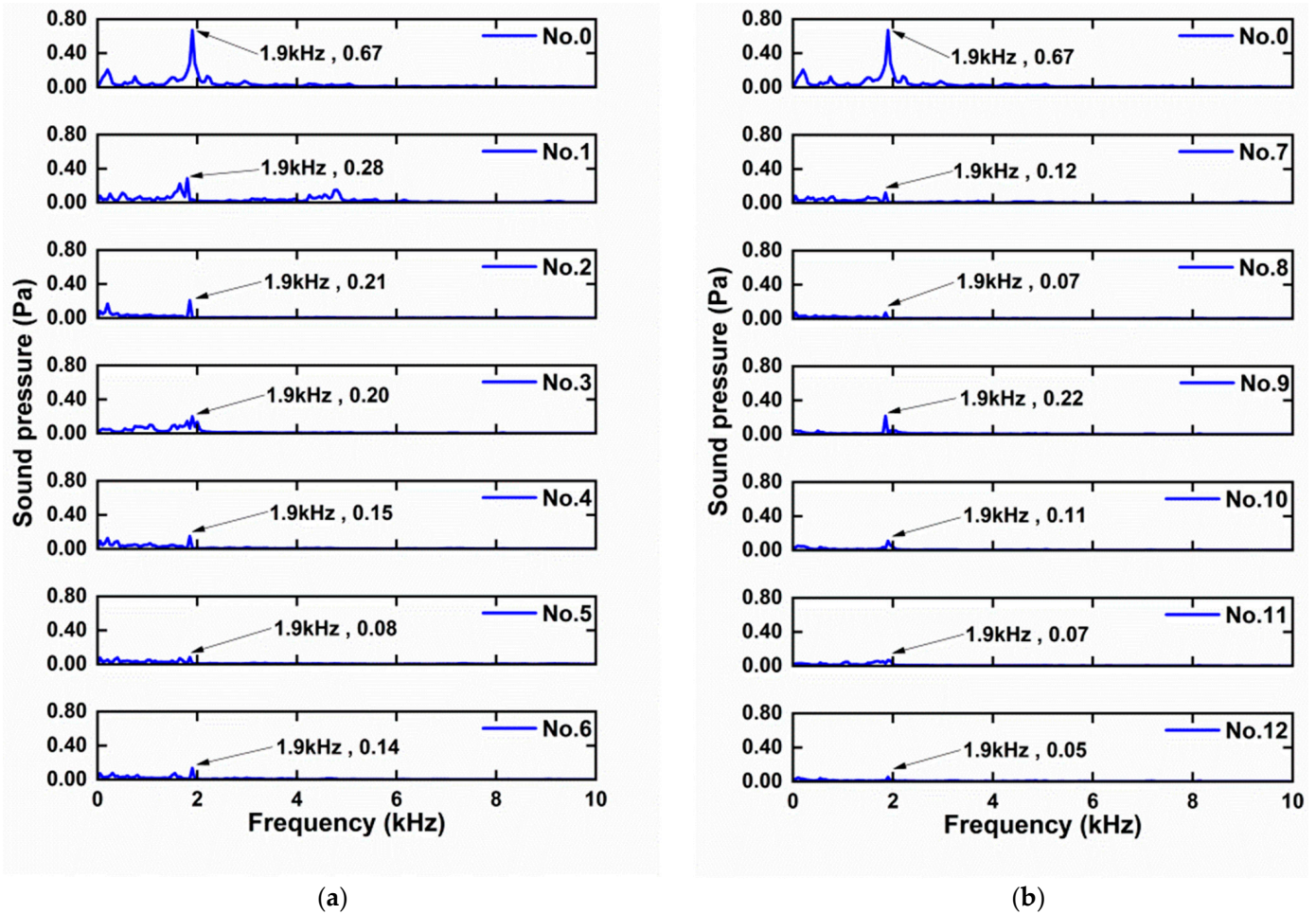


Figure 9. Frictional noise spectra of specimens. (a) Unclad specimen 0 and clad specimens 1–6; (b) unclad specimen 0 and clad specimens 7–12.

3.5. Residual Stress

Figure 10 presents the averaged residual stress on the surfaces of specimens with and without laser-clad coating, which was measured by means of a TEC 4000 X-ray diffraction system (TEC Materials Testing, Knoxville, TN, USA) prior to the tribological testing of the samples. Three different points were selected on the surface of each specimen, and the radial and tangential residual stresses with respect to the direction of rotation in the tribology tests were measured at each point. The experimental data shown in Figure 10 are the averaged values from the three points from which it can be observed that all the laser-clad specimens have compressive residual stresses in both directions, while the unclad specimen has tensile residual stresses. Specimen 11 has the largest compressive residual stresses, while specimen 12 has the second largest compressive residual stress. Specimen 10 has the smallest compressive residual stresses in both the radial and tangential directions, which may be due to the lower laser-cladding power used for this specimen.

Considering that specimens 11 and 12 have the best performance in both vibrations and noise reduction and these two specimens have larger residual compressive stresses than the other laser-clad specimens, it may be concluded that the residual compressive stress has a positive relationship with the vibration and noise reduction, i.e., a specimen with larger residual compressive stress may have better vibration- and noise-damping performance. This finding is consistent with other previous studies [30–32].

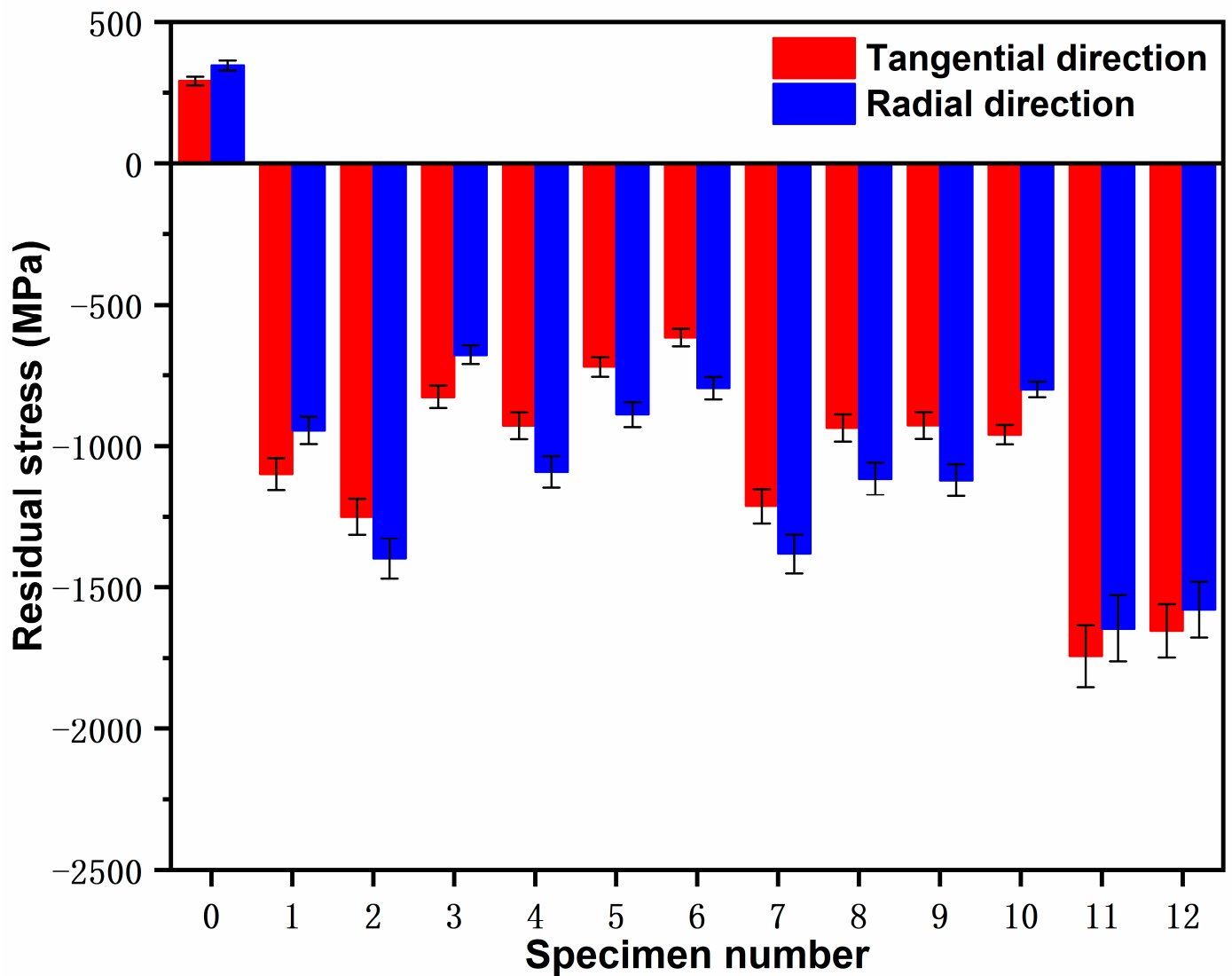


Figure 10. Average residual stresses on the surface of specimen with and without laser-clad coating.

3.6. Electrochemical Property

Figure 11 presents the polarization curves of specimens with and without a laser-clad coating obtained using the Gamry Electrochemical Station (Model Interface 1010E). It can be seen from Figure 11 that the polarization curves of all specimens are divided into two parts, namely the anodic polarization curve and the cathodic polarization curve. The anodic polarization curve corresponds to the upper part of the curve, while the cathodic polarization curve corresponds to the lower part of the curve.

The trend of the dynamic potential curves of each group is similar. For example, Figure 11a shows that the corrosion potential of the laser-clad samples is significantly higher than that of the unclad sample and that the corrosion potential of specimen 2 is the highest in the Ni35/WC coating group. Figure 11 also shows that the corrosion potentials of the Ni60/WC coating group are higher than those of other groups. Compared with the other coatings, the corrosion potential for sample 9 increases, the corrosion current density decreases, and the corrosion resistance increases.

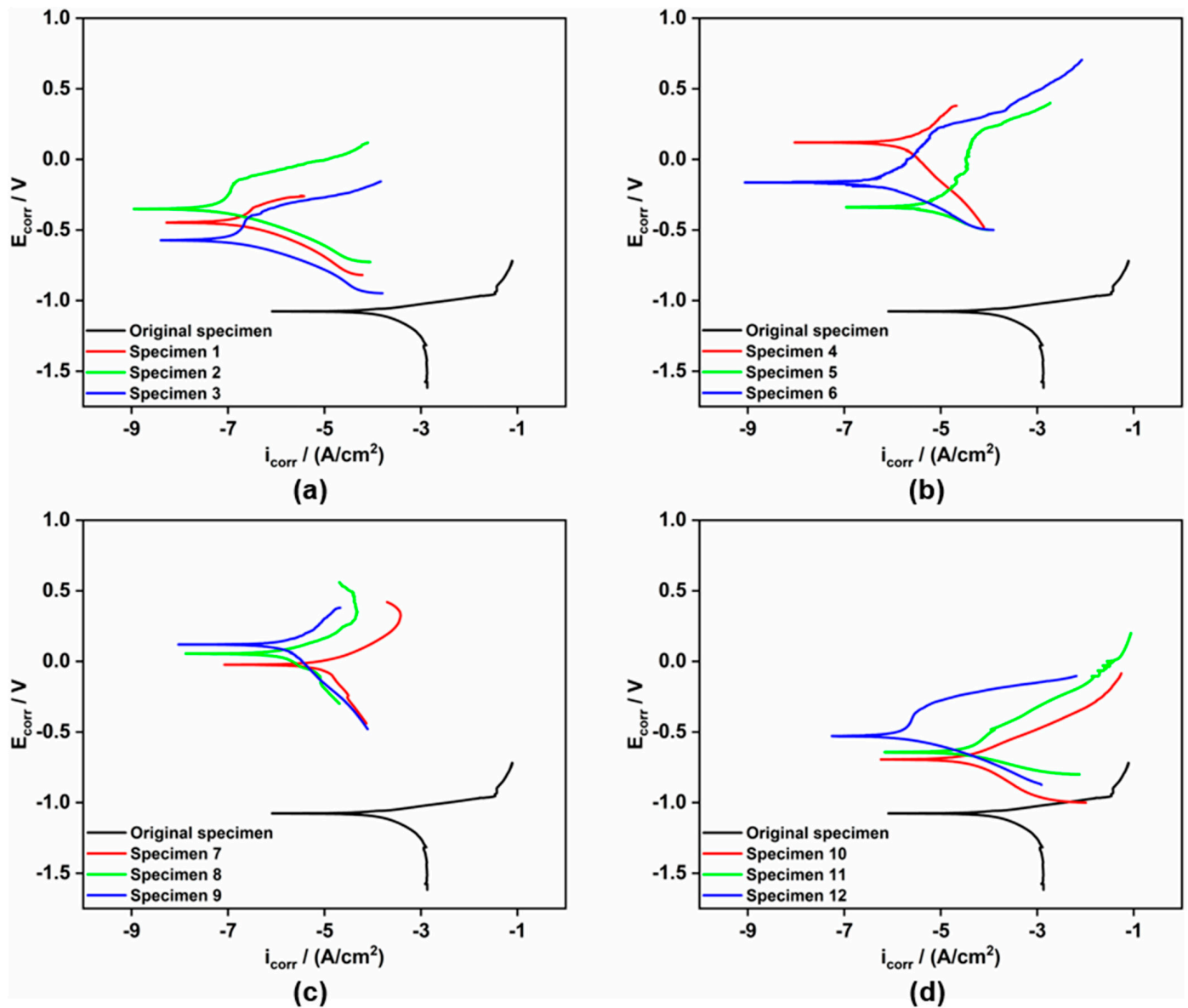


Figure 11. Polarization curve of specimens with and without laser-clad coating. (a) Specimens 0–3; (b) Specimens 0, 4–6; (c) Specimens 0, 7–9; (d) Specimens 0, 10–12.

3.7. Microstructure Analysis

3.7.1. SEM Observation

Figure 12 shows the surface topographies obtained by the SEM of the unclad specimen 0 and the 12 laser-clad specimens after the ball-on-plate tribological tests. It can be observed from Figure 12 that there are obvious fatigue failures, peeling, grooves, and abrasive wear on the surface of the unclad specimen 0. Much less fatigue failure and abrasive wear can be observed on the surfaces of the laser-clad specimens 1–12, but significant grooves were observed on the surfaces of specimens 3 and 8–12. In the groups of Ni35/WC (specimens 1–3) and Ni625/WC coatings (specimens 10–12), more serious wear can be observed on the surface of specimens 1 and 10, possibly due to the lower power used in the laser cladding for these specimens; this is consistent with the higher wear volume measured by the white light interferometer for these specimens, as shown in Figures 6 and 7.

Of the group of Ni45/WC coatings, the surface of specimen 4 appears quite rough, but it has better anti-wear performance than the other two specimens of the group because it has larger WC content, namely 40% of WC. Of the group of Ni60/WC coatings, the surface of specimen 7 is quite smooth and has better anti-wear performance than that of the other

two specimens, 8 and 9, in the group; again, this is thought to be due to the larger WC content (40%) and the larger compressive residual stress on the surface of specimen 7, as shown in Figure 10.

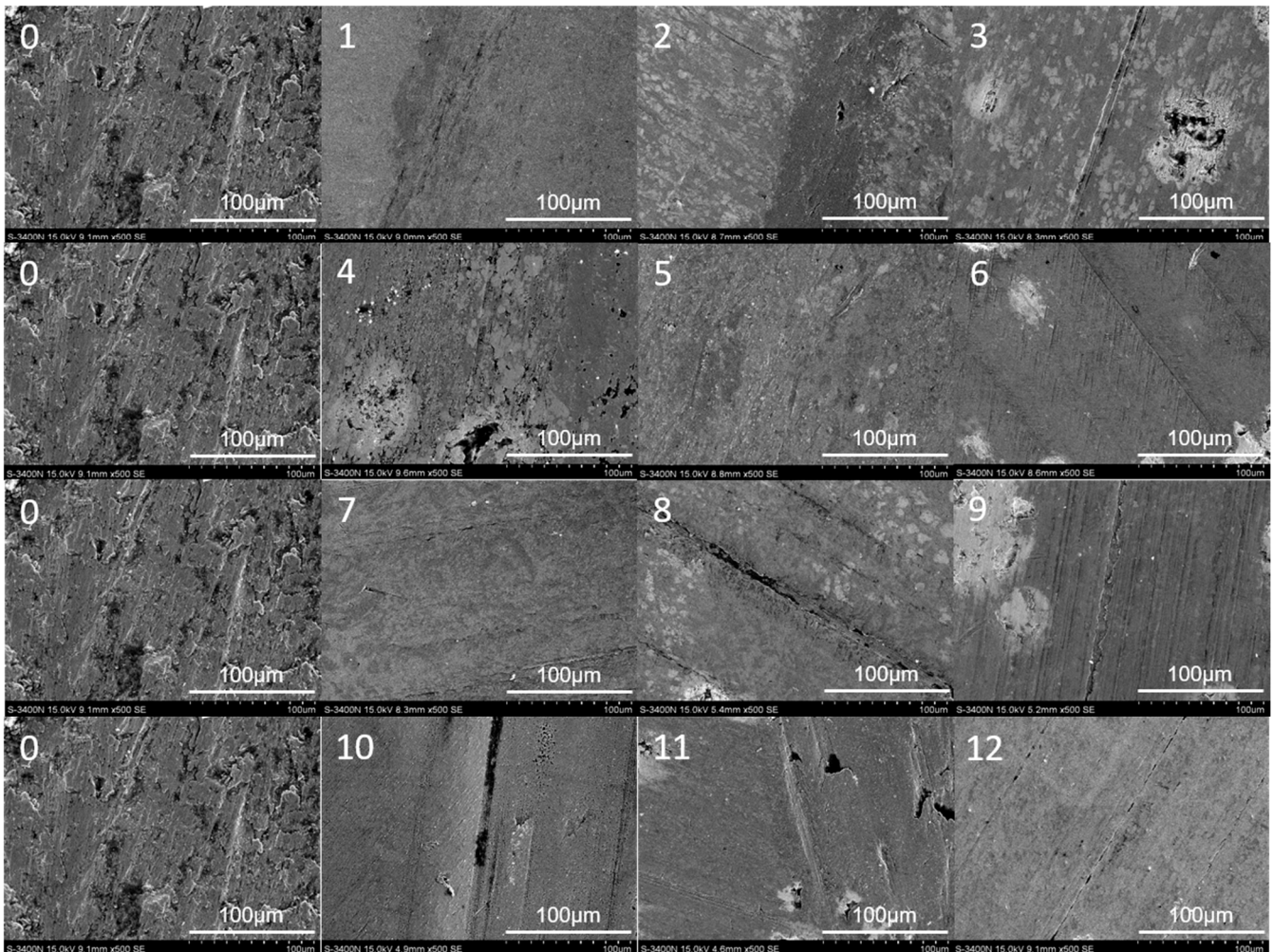


Figure 12. Surface topography of 12 laser-clad specimens after tribological tests observed by SEM under 500× magnification compared with that of unclad specimen 0 (left-hand column).

Deeper grooving is observed on specimen 10 compared with that of specimens 11 and 12, indicating that specimen 10 has worse anti-wear performance than that of the other two specimens in the same Ni625/WC coating group. This may be caused by the lower power used in the laser cladding and the smaller compressive residual stress measured on the surface of specimen 10, as shown in Figure 10.

Figure 13a,b show the surface cross-section obtained by SEM of specimens 6 and 9, respectively. Although there is some evidence of an inclusion (possibly an artifact from the specimen preparation) in the left-hand micrograph, it can be seen that the interface between the Ni/WC layer and the 316L stainless steel layer is generally smooth without any cracks or porosity, indicating the excellent quality of these laser-clad coatings.

3.7.2. XRD Analysis

It can be seen from the XRD phase plots in Figure 14 that the laser-clad layers of the selected specimens 3, 6, 9, and 12 contain multiple phases, including WC, W_2C , and FeNi. The WC particles were partially decomposed into W and C during the laser cladding process and then precipitated in reactions with Fe, Cr, Mo, and other elements to form new carbides such as Fe_5C_2 , Cr_3C_2 , and MoC. The presence of the W_2C phase is due to

the bonding from the W-rich phase during the cladding process. The proportion of Cr in specimens 9 (Ni60/WC) and 12 (Ni625/WC) is larger than that of other specimens, and more Cr-containing compounds are present, which improves not only the wear resistance but also the corrosion resistance of the laser-clad layers. In addition, a MoC phase is observed in specimens 9 and 12 that can also improve the wear resistance of the coating. With the increase in Mo content, the surface micro-cutting process is inhibited, surface peeling is reduced, and the coating is less porous and more smooth [33].

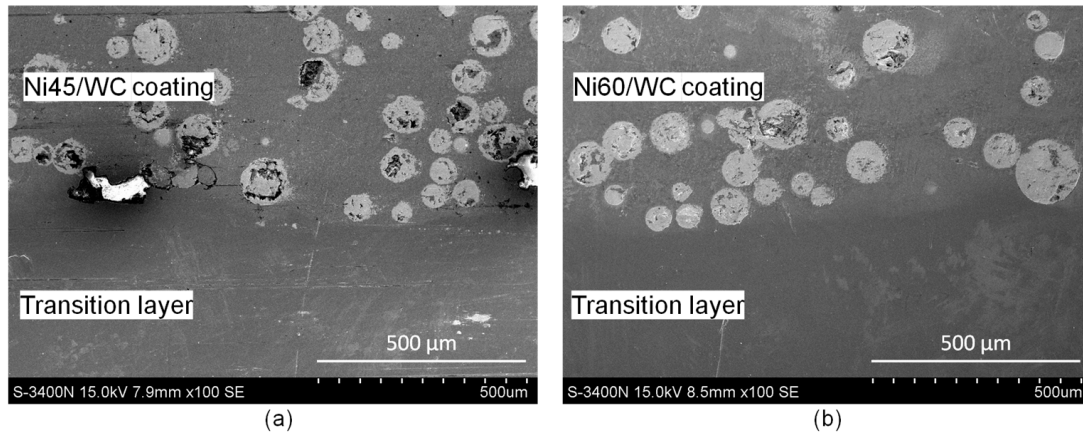


Figure 13. Cross-section of specimen laser-clad surfaces observed by SEM under 100× magnification. (a) Specimen 6; (b) Specimen 9.

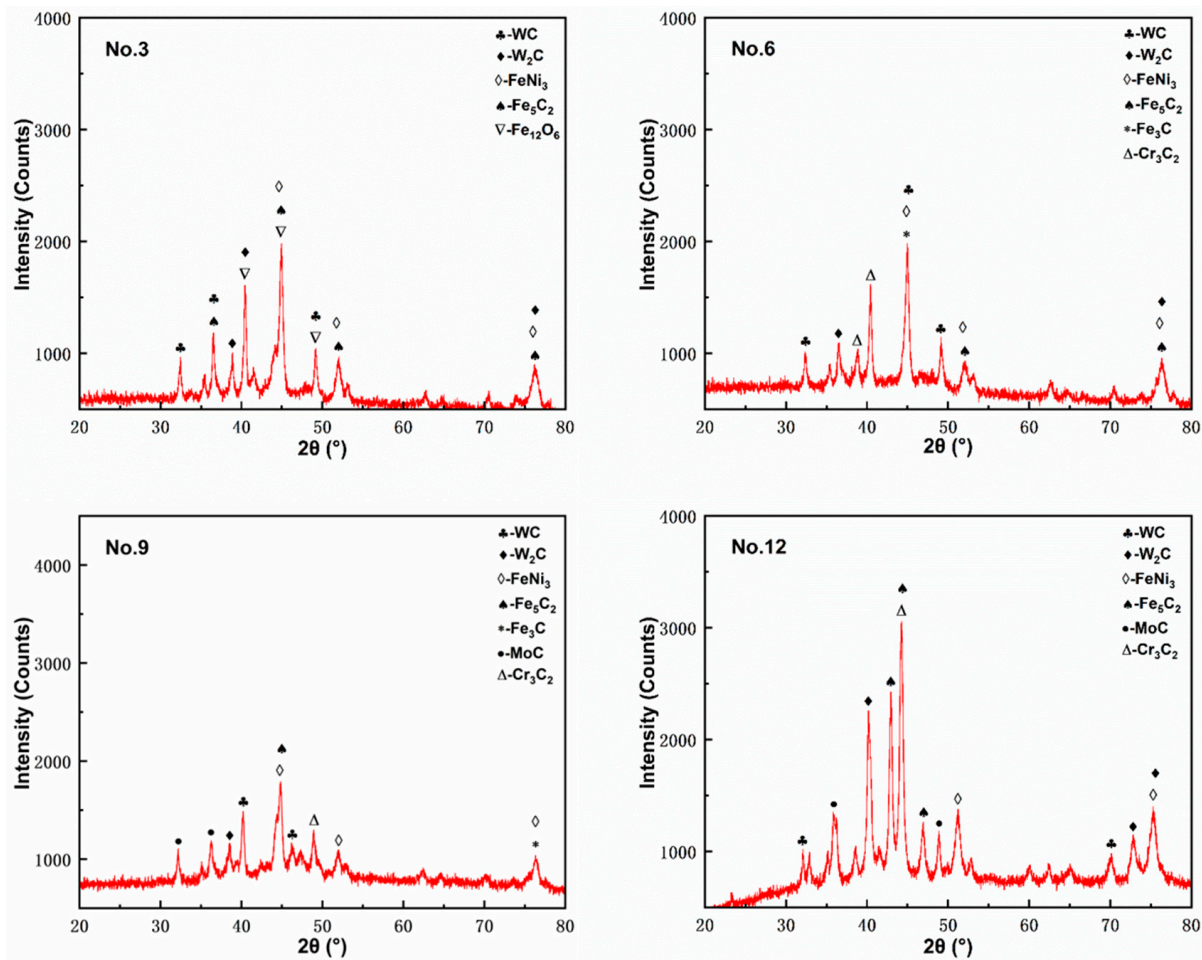


Figure 14. XRD phase analysis of the laser-clad specimens 3, 6, 9, and 12.

4. Conclusions

The tribological and mechanical properties of various laser-clad stainless steel-Ni/WC composite double-layer coatings were investigated in this study. The residual stresses on the surfaces of the coatings were measured, and the microstructures of the laser-clad layers were observed and analyzed in order to explore the mechanisms of anti-wear/corrosion and vibration/noise-damping performance enhancements. The following conclusions may be drawn from the results:

- (1) In ball-on-plate tribological testing, the COFs of all the laser-clad specimens are significantly lower and more stable than those of the specimens without laser-clad coating. Similarly, the wear rates of all the laser-clad specimens are significantly lower than those of the specimens without laser-clad coating.
- (2) Under the same tribological testing conditions, all the laser-clad specimens have excellent performance in vibration- and noise-damping compared with the unclad specimen. Specimens 10–12 with the Ni625/WC coatings have the best overall performance in both vibration and noise reduction, indicating that Ni625/WC is the best laser-cladding composite material for reducing vibration and noise effects. The Ni35/WC-clad specimens have the worst noise and vibration performance.
- (3) The corrosion potential of the laser-clad specimens is significantly increased compared with the unclad specimen, indicating that the corrosion resistance of the base material has been improved by the Ni/WC laser-cladding process. The laser-clad Ni/WC coatings are shown to contain multiple phases of WC, W₂C, FeNi, Fe₅C₂, Cr₃C₂, and MoC, which are likely to play an important role in the enhancement of the anti-corrosion properties of the laser-clad specimens. However, these initial corrosion results need to be confirmed by long-term immersion tests, exposing the clad surfaces to (say) 3.5% NaCl solution for at least 30 days.
- (4) High levels of compressive residual stresses were found in all the specimens with laser-clad coatings, which compares with the low levels of tensile residual stress measured in the unclad specimen. It is thought that these high compressive residual stresses contribute to the improvement in the anti-wear/corrosion and vibration/noise properties of the laser-clad specimens.
- (5) In this study, the Ni625/WC coatings gave the best performance in frictional vibration and noise reduction, while the Ni60/WC coatings gave the best performance in anti-wear and corrosion resistance. Generally, the coatings produced with the higher laser power settings gave improved performance. However, this performance is highly dependent on the particular laser-clad materials chosen, and further optimization of the laser-processing parameters for different materials would be desirable.

Author Contributions: Conceptualization, S.W.; methodology, S.W. and Q.S.; validation, S.W., Q.S., and R.Z.; formal analysis, R.Z.; investigation, R.Z. and Y.L.; resources, S.W. and Q.S.; data curation, S.W.; writing—original draft preparation, R.Z. and Y.L.; writing—review and editing, S.W., D.B., and M.B.; supervision, S.W. and Q.S.; project administration, S.W.; funding acquisition, S.W. and Q.S. All authors have read and agreed to the published version of the manuscript.

Funding: This research was partly funded by the Science and Technology Commission of Shanghai Municipal, grant number 18060502400, and the Natural Science Foundation of Shanghai, grant number 21ZR1445000.

Institutional Review Board Statement: Not applicable.

Informed Consent Statement: Not applicable.

Data Availability Statement: Data are contained within the article.

Conflicts of Interest: The authors declare no conflicts of interest.

References

1. Ma, H.; Liu, Z.; Li, J.; Liu, Q.; Zhang, J.; Wei, T. Optimization design of environmental-friendly Cu-Fe laser cladding coating for self-grown microchannel in a marine corrosive environment. *J. Alloys Compd.* **2023**, *940*, 168820. [[CrossRef](#)]
2. Zou, Y.; Ma, B.; Cui, H.; Lu, F.; Xu, P. Microstructure, wear, and oxidation resistance of nanostructured carbide-strengthened cobalt-based composite coatings on Invar alloys by laser cladding. *Surf. Coat. Technol.* **2020**, *381*, 125188. [[CrossRef](#)]
3. Khorram, A.; Davoodi Jamaloei, A.; Paidar, M.; Cao, X. Laser cladding of Inconel 718 with 75Cr₃C₂+25(80Ni20Cr) powder: Statistical modeling and optimization. *Surf. Coat. Technol.* **2019**, *378*, 124933. [[CrossRef](#)]
4. Caneda, C.M.; Fogagnolo, J.B.; Kiminami, C.S.; Afonso, C.R.M. Ultrafine eutectic coatings from Fe-Nb-B powder using laser cladding. *Mater. Charact.* **2020**, *160*, 110080. [[CrossRef](#)]
5. Amanov, A.; Karimbaev, R.; Berkebile, S.P. Effect of ultrasonic nanocrystal surface modification on wear mechanisms of thermally-sprayed WC-Co coating. *Wear* **2021**, *477*, 203873. [[CrossRef](#)]
6. Kumar, J.K.; Rao, T.B.; Krishna, K.R. The Microstructural properties and tribological performance of Al₂O₃ and TiN nanoparticles reinforced Ti-6Al-4V composite coating deposited on AISI304 steel by TIG cladding. *J. Tribol.* **2023**, *1*, 145. [[CrossRef](#)]
7. Zhang, C.; Pei, S.; Ji, H.; Cui, Y.; Li, M. Fabrication of Ni60-SiC coating on carbon steel for improving friction, corrosion properties. *Mater. Sci. Technol.* **2017**, *33*, 446–453. [[CrossRef](#)]
8. Tian, Z.-H.; Zhao, Y.-T.; Jiang, Y.-J.; Ren, H.-P. Microstructure and properties of Inconel 625 + WC composite coatings prepared by laser cladding. *Rare Met.* **2021**, *40*, 2281–2291. [[CrossRef](#)]
9. Wang, X.H.; Liu, S.S.; Zhang, M.; Qu, K.L. Effect of rare earth oxide on the microstructure and wear properties of in situ-synthesized ceramics-reinforced Fe-based laser cladding coatings. *Tribol. Trans.* **2020**, *63*, 345–355. [[CrossRef](#)]
10. Wang, G.; Wang, S.; Yin, Z.; Yang, X.; Wen, D.; Sun, Y. Synthesis of Ni-WC/Al-Ni functionally graded coating with advanced corrosion and wear resistance on AZ91D Mg alloy by laser cladding. *Mater. Lett.* **2023**, *333*, 133645. [[CrossRef](#)]
11. Arias-González, F.; del Val, J.; Comesaña, R.; Penide, J.; Lusquiños, F.; Quintero, F.; Riveiro, A.; Boutinguiza, M.; Pou, J. Fiber laser cladding of nickel-based alloy on cast iron. *Appl. Surf. Sci.* **2016**, *374*, 197–205. [[CrossRef](#)]
12. Chen, Y.; Zhang, Q.; Chen, Z.; Wang, L.; Yao, J.; Kovalenko, V. Study on the element segregation and Laves phase formation in the carbon nanotubes reinforced IN718 superalloy by laser cladding. *Powder Technol.* **2019**, *355*, 163–171. [[CrossRef](#)]
13. Zhang, M.; Luo, S.X.; Liu, S.S.; Wang, X.H. Effect of molybdenum on the wear properties of (Ti,Mo)C-TiB₂-Mo₂B particles reinforced Fe-based laser cladding composite coatings. *J. Tribol.* **2018**, *140*, 051603. [[CrossRef](#)]
14. Liu, Y.P.; Liang, Y.L.; Fu, H.G. Improvement properties of laser cladding Ni45-Cr₃C₂ coatings by adding B₄C and V. *Mater. Sci. Technol.* **2023**, *39*, 443–453.
15. Jiang, D.; Cui, H.; Zhao, X.; Chen, H.; Ma, G.; Song, X. Beneficial effects of Co to CoCrNiMoCB coatings obtained by laser cladding. *Mater. Lett.* **2022**, *323*, 132558. [[CrossRef](#)]
16. Yuan, S.H.; Li, H.L.; Han, C.F.; Li, W.Q.; Xu, X.F.; Chen, C.; Wei, R.; Wang, T.; Wu, S.J.; Li, F.S. FeCoNiCrAl_{0.6} high-entropy alloy coating on Q235 steel fabricated by laser cladding. *Mater. Sci. Technol.* **2023**, *39*, 705–713. [[CrossRef](#)]
17. Wang, T.Y.; Zhao, M.X.; Li, Z.; Wang, X.N.; Wei, J.C. Effect of indium on the microstructure and corrosion resistance of the galvanising coating. *Mater. Sci. Technol.* **2023**, *39*, 767–776. [[CrossRef](#)]
18. Riquelme, A.; Escalera-Rodriguez, M.D.; Rodrigo, P.; Rams, J. Role of laser cladding parameters in composite coating (Al-SiC) on aluminum alloy. *J. Therm. Spray Technol.* **2016**, *25*, 1177–1191. [[CrossRef](#)]
19. Teixeira, M.F.; Pacheco, J.T.; da Silva, L.J.; Rabelo, A.; Pereira, M.; Niño, C.E. Laser cladding of Metco 1040[®] (Fe-V-Mn-C) on Hadfield steel: Effect of processing parameters on microstructure and wear resistance. *Opt. Laser Technol.* **2021**, *142*, 107219. [[CrossRef](#)]
20. Mahade, S.; Awe, S.A.; Björklund, S.; Lukáč, F.; Mušálek, R.; Joshi, S. Sliding wear behavior of a sustainable Fe-based coating and its damage mechanisms. *Wear* **2022**, *500–501*, 204375. [[CrossRef](#)]
21. Tonolini, P.; Montesano, L.; Pola, A.; Landriani, E.; Gelfi, M. The effect of laser-cladding on the wear behavior of gray cast iron brake disc. *Procedia Struct. Integr.* **2021**, *33*, 1152–1161. [[CrossRef](#)]
22. Manoj, A.; Saurabh, A.; Narala, S.K.R.; Saravanan, P.; Natu, H.P.; Verma, P.C. Surface modification of grey cast iron by laser cladding for automotive brake disc application. *Wear* **2023**, *532–533*, 205099. [[CrossRef](#)]
23. Ouyang, C.; Wang, R.; Zhao, C.; Wei, R.; Li, H.; Deng, R.; Bai, Q.; Liu, Y. Multi-layer laser cladding analysis and high-temperature oxidative wear behavior of cast iron with a low expansion coefficient. *Surf. Coat. Technol.* **2023**, *474*, 130079. [[CrossRef](#)]
24. Li, Y.J.; Dong, S.Y.; Yan, S.X.; Li, E.Z.; Liu, X.T.; He, P.; Xu, B.S. Deep pit repairing of nodular cast iron by laser cladding NiCu/Fe-36Ni low-expansion composite alloy. *Mater. Charact.* **2019**, *151*, 273–279. [[CrossRef](#)]
25. Liu, J.; Liu, H.; Tian, X.; Yang, H.; Hao, J. Microstructural evolution and corrosion properties of Ni-based alloy coatings fabricated by multi-layer laser cladding on cast iron. *J. Alloys Compd.* **2020**, *822*, 153708. [[CrossRef](#)]
26. Wang, S.W.; Liao, Y.H.; Wang, T.D. Properties of vibration and noise reduction and friction/wear performance of laser clad Ni625/WC coatings. *China Surf. Eng.* **2021**, *34*, 94–103.
27. Yuan, W.; Li, R.; Chen, Z.; Gu, J.; Tian, Y. A comparative study on microstructure and properties of traditional laser cladding and high-speed laser cladding of Ni45 alloy coatings. *Surf. Coat. Technol.* **2021**, *405*, 126582. [[CrossRef](#)]
28. Chen, Y.; Cui, H.; Li, L.; Song, X.; Feng, Y.; Zhang, C.; Huang, W. Effect of WC incorporation on the microstructure and mechanical properties of Ni625/WC spark plasma sintered composites. *Ceram. Int.* **2024**, *50*, 16987–16997. [[CrossRef](#)]

29. Morin, L.; Braham, C.; Tajdary, P.; Seddik, R.; Gonzalez, G. Reconstruction of heterogeneous surface residual-stresses in metallic materials from X-ray diffraction measurements. *Mech. Mater.* **2021**, *158*, 103882. [[CrossRef](#)]
30. Zhu, D.P.; Yu, X.K.; Sai, Q.Y.; Wang, S.W.; Barton, D.; Fieldhouse, J.; Kosarieh, S. Noise and vibration performance of automotive disk brakes with laser-machined M-shaped grooves. *Proc. Inst. Mech. Eng. Part D* **2023**, *237*, 978–990.
31. Wang, S.; Yan, S.; Lin, J.; Batako, A.D. Study on the effects of laser quenching power and scanning speed on the property of cast iron. *J. Phys. Conf. Ser.* **2022**, *2198*, 012050. [[CrossRef](#)]
32. Wang, S.W.; Guo, W.; Zeng, K.; Zhang, X.G. Characterization of automotive brake discs with laser-machined surfaces. *Automot. Innov.* **2019**, *2*, 190–200. [[CrossRef](#)]
33. Cui, G.; Han, W.; Zhang, W.; Li, J.; Kou, Z. Friction and wear performance of laser clad Mo modified Stellite 12 matrix coatings at elevated temperature. *Tribol. Int.* **2024**, *196*, 109738. [[CrossRef](#)]

Disclaimer/Publisher’s Note: The statements, opinions and data contained in all publications are solely those of the individual author(s) and contributor(s) and not of MDPI and/or the editor(s). MDPI and/or the editor(s) disclaim responsibility for any injury to people or property resulting from any ideas, methods, instructions or products referred to in the content.